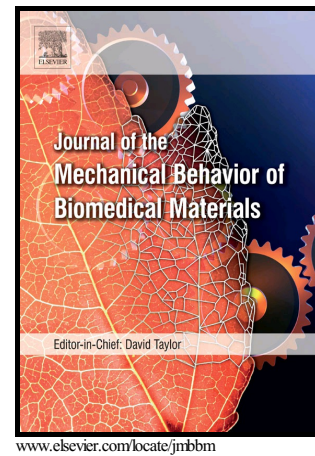


Author's Accepted Manuscript

Importance of Asymmetry and Anisotropy in Predicting Cortical Bone Response and Fracture Using Human Body Model Femur in Three-Point Bending and Axial Rotation

F. Khor, D.S. Cronin, B. Watson, D. Gierczycka, S. Malcolm



PII: S1751-6161(18)30320-5
DOI: <https://doi.org/10.1016/j.jmbbm.2018.07.033>
Reference: JMBBM2901

To appear in: *Journal of the Mechanical Behavior of Biomedical Materials*

Received date: 14 March 2018
Revised date: 9 June 2018
Accepted date: 23 July 2018

Cite this article as: F. Khor, D.S. Cronin, B. Watson, D. Gierczycka and S. Malcolm, Importance of Asymmetry and Anisotropy in Predicting Cortical Bone Response and Fracture Using Human Body Model Femur in Three-Point Bending and Axial Rotation, *Journal of the Mechanical Behavior of Biomedical Materials*, <https://doi.org/10.1016/j.jmbbm.2018.07.033>

This is a PDF file of an unedited manuscript that has been accepted for publication. As a service to our customers we are providing this early version of the manuscript. The manuscript will undergo copyediting, typesetting, and review of the resulting galley proof before it is published in its final citable form. Please note that during the production process errors may be discovered which could affect the content, and all legal disclaimers that apply to the journal pertain.

Importance of Asymmetry and Anisotropy in Predicting Cortical Bone Response and Fracture Using Human Body Model Femur in Three-Point Bending and Axial Rotation

F Khor¹, DS Cronin^{1*}, B Watson¹, D Gierczycka¹, S Malcolm²

¹Department of MME, University of Waterloo, 200 University Avenue West, Waterloo, Canada

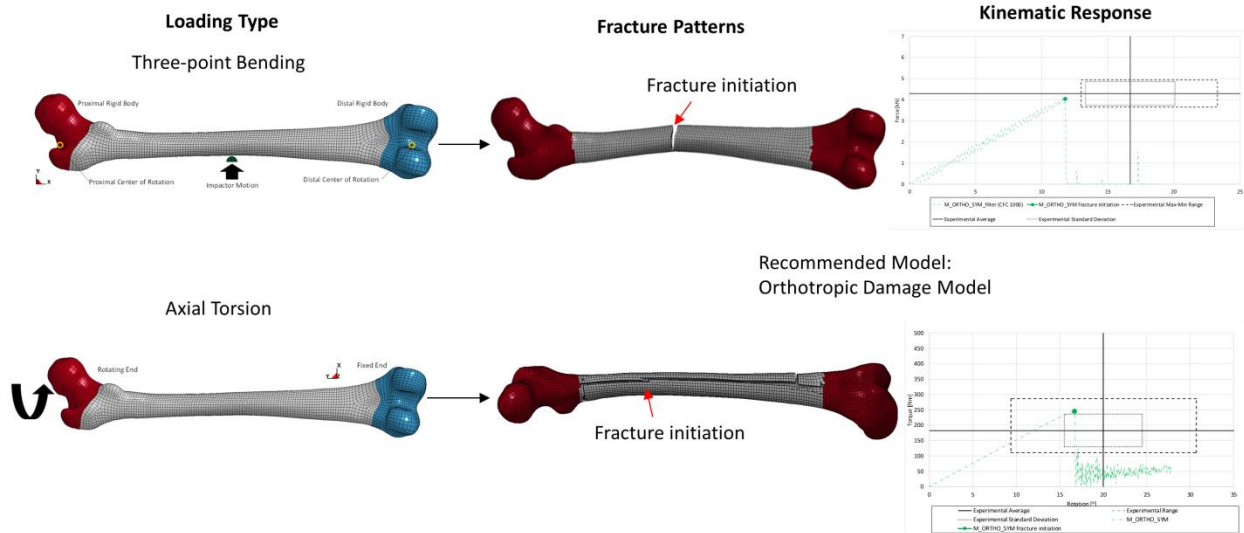
²Honda R&D Americas, Raymond, Ohio, USA

*Corresponding Author: Dr. Duane Cronin Department of Mechanical Engineering University of Waterloo 200 University Ave. West Waterloo, Ontario, Canada, N2L 3G1 (519) 888-4567 x32682, dscronin@mecheng1.uwaterloo.ca

Abstract:

Modeling of cortical bone response and failure is critical for the prediction of Crash Induced Injuries (CII) using advanced finite element (FE) Human Body Models (HBM). Although cortical bone is anisotropic and asymmetric in tension and compression, current HBM often utilize simple isotropic, symmetric, elastic-plastic constitutive models. In this study, a 50th percentile male femur FE model was used to quantify the effect of asymmetry and anisotropy in three-point bending and axial torsion. A complete set of cortical bone mechanical properties was identified from a literature review, and the femur model was used to investigate the importance of material asymmetry and anisotropy on the failure load/moment, failure displacement/rotation and fracture pattern. All models were able to predict failure load in bending, since this was dominated by the cortical bone material tensile response. However, only the orthotropic model was able to predict the torsional response and failure moment. Only the orthotropic model predicted the fracture initiation location and fracture pattern in bending, and the fracture initiation location in torsion; however, the anticipated spiral fracture pattern was not predicted by the models for torsional loading. The results demonstrated that asymmetry did not significantly improve the prediction capability, and that orthotropic material model with the identified material properties was able to predict the kinetics and kinematics for both three-point bending and axial torsion. This will help to provide an improved method for modeling hard tissue response and failure in full HBM.

Graphical Abstract:



Keywords:

hard tissue, constitutive model, fracture pattern, femur, human body model, finite element model

1. Introduction and Background

Human Body Models (HBMs) provide a computational platform to assess occupant response and the potential for injury in crash scenarios [Gierczycka et al., 2015; Schmitt, 2014], and, ultimately, to mitigate injury. An important goal for HBMs has been to predict injury at the tissue level and, in particular, to predict hard tissue failure or bone fracture, as this is often an injury of importance [AIS, 2005], or may be indicative of nearby soft tissue injuries [Tscherne et al., 1982]. However, the capability of HBMs to predict hard tissue fracture has been limited by the use of relatively simple constitutive models, for example isotropic metals plasticity models in the Global Human Body Models Consortium (GHBM) and Total Human Model for Safety (THUMS) models, coupled with erosion-based material failure approaches [Hambli et al., 2012, 2013]. The mechanical behavior of bone and the mechanism of bone fracture have been investigated using computational models at the microscopic and macroscopic

levels for over 40 years [Zysset et al., 2013]. Nevertheless, a widely accepted continuum treatment for cortical bone that can predict the failure load and fracture pattern for different modes of loading is not yet available.

Predicting fracture propagation and fracture pattern will enable HBMs to better predict the potential for injury in impact scenarios and could potentially enable HBMs to predict post-fracture response, which is acknowledged to present challenges in existing HBMs [DeWit et al., 2012]. In the short term, accurate prediction of cortical bone response and potential for failure is critical for HBM to address current challenges in human safety. Although mechanical testing of bone has identified asymmetry and anisotropy in bone material, the importance of these effects has not been assessed in full HBMs, where computational robustness and efficiency through a relatively coarse finite element mesh size are required.

This study aims to narrow that gap by identifying a set of cortical bone material properties from experimental studies and assessing the contribution of asymmetry and anisotropy to failure load and fracture pattern using a three-dimensional femur bone model from a current HBM assessed with independent whole-bone experimental data.

1.1 Mechanical Response and Modeling of Bone

The complex hierarchical structure of bone has been associated with anisotropic material properties, asymmetry in compression and tension loading, and variations in properties with deformation rate [Cowin et al., 2001; Hansen et al., 2008; McElhaney, 1966; Reilly and Burstein, 1975; Turner, 2006]. Although many reported properties exist for human and animal cortical bone, a single set of properties has not yet been proposed for general use for three-dimensional bone models in HBMs.

Many studies have investigated hard tissue constitutive models at the coupon level [Fondrk et al., 1999; Garcia et al., 2009, 2010; Iwamoto, 2005; Schileo et al., 2008; Tanaka et al., 2012; Zysset et al., 2013], but these approaches have not been translated to three-dimensional bone models in HBMs. The proposed constitutive models included a linear elastic-plastic formulation for low strain rates in the physiological range [Garcia et al., 2009, 2010; Tanaka et al., 2012;], a non-linear visco-elastoplasticity formulation for a large strain deformation and higher strain rates [Fondrk et al., 1999], anisotropy [Iwamoto et al., 2005], a compression-tension asymmetry [Iwamoto et al., 2005; Niebur et al., 2000; Schileo et al., 2008], and a post-yield damage [Zysset et al., 2013]. Two studies [Iwamoto et al., 2005, Martin et al., 1998] identified the bone strength asymmetry and anisotropy as the main contributors to bone fracture mechanisms and patterns. However, current methods of simulating cortical bone in HBMs treat the bone material as isotropic, with symmetric compression and tension properties modeled using metal plasticity approaches [e.g. Untaroiu, 2013].

Due to the complex geometry of bones and the need for computational efficiency in HBMs, continuum-level models with element sizes on the order of 1 mm to 3 mm are used. Asgharpour et al. [2014] extracted a femur from the THUMS HBM and developed a bone material model to replicate an experimental femur bending response; however, the mesh size dependency of the predicted response limited application of the material model proposed by Asgharpour (2014) in other HBMs. In addition, strain rate dependent mechanical properties significantly over predicted the failure load (7 kN compared to an average failure force of 4.3 kN in the experiments [Funk et al., 2004]) for dynamic three-point bending of the femur. In a similar study, Untaroiu (2013) did not include rate effects in the material properties, since these properties were not consistently supported by the experimental data. He used an isotropic model with an effective plastic strain failure criterion but disabled the failure criterion in the

area in which the impactor contacted the femur to avoid failure in the compression region, and predicted a failure force of 3.82 kN in three-point bending.

Model geometric simplifications have also been proposed, such as a two-dimensional (2D) femoral neck model [Hambli et al., 2012], with a clear limitation that it could only be applied to relatively simple loading, where a plane stress assumption incorporated in Hambli's [2012] model could not be applied to three-dimensional HBMs. Furthermore, Hambli [2012] implemented the material damage and crack propagation as a user-defined constitutive model, which is at present not available to other researchers. In another study, Hambli et al. [2013] studied the quasi-static three-point bending load of a single trabeculae strut using a 2D finite element (FE) model with a user-defined material model. These methods involved a large computational cost, they are not generally available to the research community, and at present are not directly applicable in full HBMs with complex geometry.

Hard Tissue Failure

Modeling of hard tissue failure comprises two events: the accumulation of damage and initiation of the fracture, and fracture propagation. Micro-models with element sizes on the order of 1 μm have been used to investigate crack deflection into cement lines and resistance to crack propagation across osteons [Mischinski et al., 2011], which was found to decrease with increasing strain rate [Ural et al., 2011]. Methods utilized to predict fracture at the continuum level include the cohesive zone model (CZM) [Ural et al., 2011], a reduced stiffness approach [Hambli, 2013], an extended finite element (X-FEM) approach [Abdel-Wahab et al., 2012; Feerick et al., 2013; Li et al., 2013], and the element deletion or erosion approach [Hambli et al., 2012; Harrison et al., 2013]. The main limitation of the CZM is a requirement to pre-define the fracture path for the analysis [Ali et al., 2014; Feerick et al., 2013].

Although the X-FEM approach is desirable to model crack propagation, it is computationally expensive and currently applicable in 2D models [Abdel-Wahab, 2012; Feerick, 2013; Hambli, 2013; Li, 2012]. Furthermore, in a study that incorporated X-FEM in a 2D cortical bone model, simulation convergence and numerical stability presented challenges, due to multiple, mutually intersecting cracks predicted over a small region after a mesh refinement [Idkaidek et al., 2016]. Therefore, a smaller FE mesh requires a smaller time increment, leading to a longer simulation time, but without providing a guarantee of a more accurate result compared to a coarser mesh. Only a few studies [Ali et al., 2014; Giambini et al., 2016] have incorporated the X-FEM approach in 3D models, since this approach requires a custom solver and methods that are not commercially available at present.

While the element deletion (erosion) method is widely used to model material failure, one limitation is an aggregated treatment of crack initiation and propagation [Hambli et al., 2012, 2013]. The fracture pattern is thus determined by the deleted elements of the mesh. In a more geometrically complex scenario, a study by De Wit and Cronin [2012] demonstrated that a relatively simple isotropic metal plasticity model with element erosion could predict the onset of failure, but generally did not predict the fracture pattern when a maximum plastic strain erosion criterion was used. The element erosion method has been shown to predict fracture patterns at the whole-bone level [Niebur et al., 2000; Schileo et al., 2008] for some modes of loading. A strain-based failure criterion is generally employed for numerical stability [De Wit and Cronin, 2012], and was justified by Nalla et al. (2003), who demonstrated experimentally that the local criterion for fracture in human cortical bone was consistent with a strain-based criterion used in theoretical and computational bone models.

1.3 Experimental Data for Model Assessment

Evaluation of a computational model requires an objective assessment alongside the experimental data, in this case focused on cortical bone response and failure for whole-bone scenarios. The human femur is one of the most widely tested whole bones, and has been tested at the material level extensively, owing to the size of the bone and therefore the ability to extract test samples. Whole femur experimental tests include three-point bending, axial torsion and axial compression. Although axial compression loading is an important load case in vehicle crash scenarios due to interaction of the knee with the vehicle instrument panel, early investigations identified that the predicted response and failure were directly linked to the mesh transition between the diaphysis and epiphysis in the femur model. Therefore, an objective evaluation of the cortical bone material properties with this load case was not possible. Thus, three-point bending was used to assess tension-compression properties, while axial torsion was used to evaluate shear material properties.

Butterfly or tension wedge fractures are a typical fracture pattern in bending [Kress et al., 1995; Sharir et al., 2008; Turner, 2006] (Figure 1), although other patterns, such as oblique and transverse fractures, have also been identified in experiments [Kress et al., 1995; Rich, 2005]. The location of failure initiation in bending of the long bone is reported to occur on the tension side of the bone. As the crack propagates transversely across the bone and into the compressive loading regime, it often bifurcates at an angle of approximately 45 degrees to the transverse direction [Sharir et al., 2008; Turner, 2006]. The measured failure load for a human femur in three-point bending experiments ranges from 2300 N to 5800 N, depending on the gender and the loading direction (antero-posterior or medio-lateral) [Funk et al., 2004; Kennedy et al., 2004; Kress et al., 1993; Mather et al., 1967].

In contrast, a distinctive spiral fracture pattern is observed for axial torsion loading in which the fracture propagates perpendicular to the orientation of the maximum principal stress [Martin, 2015], with the failure initiation occurring at the mid-shaft of the bone [Porta et al., 1997; Rich et al., 2005]. The reported axial torque at failure ranges from 108 Nm to 183 Nm [Kress et al., 1993; Martens et al., 1980].

2. Methods

A three-dimensional femur finite element (FE) model (Figure 2) was isolated from a current 50th percentile male Human Body Model (HBM) (GHBMC M50, Version 4.3, GHBMC.org) and subjected to two load cases using a commercial FE software (LS-Dyna R7.1.2, LSTC, Livermore CA). The methodology included an identification of material properties from the literature, selection of two constitutive models to represent the material properties, a single element verification of the constitutive models, and quantification of the material anisotropy and asymmetry using the whole-bone femur model.

2.1 Identification of Cortical Bone Mechanical Properties

Although many studies have measured one or more of the bone mechanical properties independently [Ashman et al., 1984; Currey, 2002; Gibson et al., 1988; Hansen et al., 2008; Reilly & Burstein, 1974; Tang et al., 2015], no single human cadaver tissue study has fully characterized all relevant mechanical properties of cortical bone for use in FE models (Young's, shear and bulk moduli, Poisson's ratio in all directions, and strength/damage in tension, compression and shear modes of loading). The cortical bone elastic mechanical properties (Table 1) and strength properties (Table 2) were identified from four

studies: tension and compression properties were taken from Reilly and Burstein, [1974, 1975], shear properties were determined from Tang et al. [2015], while the Poisson's ratio was provided by Ashman et al. [1984]. Properties from these studies were utilized due to the extensive number of experimental specimens [Reilly and Burstein, 1974, 1975], and specific modes of loading [Tang et al., 2015]. Strain rate effects were not considered in this study, since they were not supported by the whole-bone experimental data as presented in the discussion. In comparison with the current properties in the GHBM model, the Young's modulus in the current study was 18% higher, while the ultimate strength was the same in tension and 20.5% higher in compression.

2.2 Constitutive Model Identification

The reference material model currently used in the GHBM HBM for the femur cortical bone was an isotropic metal plasticity model (M_ISO_SYM) (Table 3), using the tension-based properties (Tables 1 and 2). The M_ISO_SYM model was symmetric in tension and compression. No single commercially available material model incorporated all of the desired characteristics including: anisotropy, tension-compression asymmetry for the modulus and strength, and material failure. Therefore, two available constitutive models identified from a previous, extensive survey of available constitutive models for cortical bone [Khor et al., 2016a; 2016b] were used to investigate asymmetry (M_ISO_ASYM) and anisotropy (M_ORTHO_SYM) (Table 3).

The M_ISO_ASYM did not include anisotropy and therefore only the tension-compression properties in the longitudinal (osteon) direction [Reilly and Burstein, 1974] were utilized. In the case of the M_ORTHO_SYM model, the material directions were specified at the element level based on node numbering to ensure the material axes followed the contour of the bone. The material was treated as orthotropic with the 1-direction corresponding to the osteon longitudinal or length direction, and following the long axis of the whole bone. The 2-direction corresponded to the transverse (circumferential) direction, while the 3-direction was defined through-thickness (radial). Since the M_ORTHO_SYM model did not incorporate tension-compression asymmetry for the elastic moduli, the tension-based elastic properties were used in the longitudinal and transverse directions (Tables 1 and 2). This choice was based on the finding that failure initiated on the tensile side of the bone in bending [Kress et al., 1995; Sharir, 2008], and the tensile strength was lower than the compressive strength. The simplified damage model definition in the M_ORTHO_SYM model was based on the definition of yield strain, namely the strain at which damage initiates, on the critical damage value, and the ultimate failure strain. The critical damage value was optimized so to match the ultimate failure stress to the experimental values [Reilly and Burstein, 1974, 1975].

All constitutive models were verified using the same isotropic and symmetric material properties (Table 3) within the models to confirm that the response was the same as the baseline material model (M_ISO_SYM). This was found to be the case, confirming that the implementation and use of the material models was as intended

Secondly, each of the material models was verified using a single element simulation for three modes of loading: tension, compression and shear (Appendix A, Figure A.1 and Figure A.2). The mechanical properties for the models (Tables 1 and 2) were incorporated with a failure criterion using the tensile plastic strain of 0.0235 [Reilly and Burstein et al., 1975].

2.3 Femur Computational Model to Assess Material Constitutive Models

Whole-bone simulations of experimental tests were undertaken using a recent HBM femur model (M50 GHBM model, Version 4.3) (Figure 2). The cortical bone in the diaphysis of the femur was meshed with linear selectively reduced fully integrated solid hexahedral elements, with three elements through the thickness. The trabecular bone (epiphysis and metaphysis) was meshed with hexahedral solid elements, while the thin cortical shell in these locations was meshed with shell elements for computational efficiency. For the purposes of this study, the epiphysis and metaphysis compliance and geometry were important. However, in all experimental cases considered, failure occurred in the diaphysis, therefore the investigated constitutive models were applied to the cortical bone solid elements in the diaphysis.

Experimental data for three-point bending and torsional experiments used in this study were derived from studies by Funk et al. [2004] and Martens et al. [1980] respectively (Table 4) because these studies provided a very detailed test set-up description, which was essential for replication of the test boundary conditions in the simulation. The length and area of the femur used in this study were in good agreement with the anthropometric data of the PMHS bone donors in the bending experiment [Funk, 2004] (Table 5). Martens et al., (1980) did not provide geometrical data on the individual femur dimensions but did report an age range of 27 to 80 years old for the femur specimens, and a mixed gender of male and female donors. To simulate the medio-lateral three-point bending test by Funk et al. [2004], a 12 mm semi-cylindrical deformable solid mesh was created for the impactor, with a rigid shell backing and steel material properties (Figure 3A). A prescribed motion was imposed on the rigid shell backing corresponding to translation in the lateral-medial direction (+‘Y’ in model axis) at a constant velocity as in the experiment conducted by Funk et al. (2004). The proximal end was constrained to only allow translation in the model ‘X’ direction whereas the distal end of the bone was constrained in all directions, and the rotations were constrained to allow rotation only about the medio-lateral direction (model ‘Z’ direction). The boundary conditions were applied to the shell mesh of the cortical bone portion of the epiphyses, representing the experimental boundary condition where the ends of the bones were potted in bone cups. The center of rotation was specified to be coincident with axis of rotation in the experiments. The responses were filtered using a CFC 1000 filter [Funk, 2004].

In the torsion experiments conducted by Martens et al. [1980], the epiphyseal ends were imbedded in rectangular blocks of plastic, which were in turn secured in the grips of a torsion testing machine. Boundary conditions were applied at the epiphyses of the femur to create torsional loading of the bone in the simulation. In this case, the long axis of the shaft was aligned with the model ‘Y’ axis (Figure 3B). The distal epiphysis was fixed in all translation and rotation directions, while the proximal epiphysis was allowed to rotate and translate about the superior-inferior direction (model ‘Y’ direction). It was not clear from the experimental study if axial translation was restricted during testing; however, a comparison of models with and without this constraint showed little difference in the torque-rotation response and fracture pattern. Therefore, axial translation was allowed, since this was the likely case in the experimental study. A prescribed motion of the proximal epiphysis was imposed about the model ‘Y’ axis, with a rotational velocity of 500 °/s after an initial ramp time of roughly 10 ms, simulating the loading time in the experimental study.

The local material coordinate system was assigned to each finite element based on the element node numbering. Although several approaches were possible (e.g. using a global vector to assign directions), the mesh and elements generally followed the principal directions of the bone: osteon, radial and transverse. Within the model, the elements were intentionally numbered in a consistent fashion using a software program (Hypermesh, Altair), such that the first two nodes of the element were

used to define the osteon direction, defining the first material direction. Within the specific FE solver, the remaining element nodes were used to define the transverse (circumferential) and radial directions. These directions were used by the material model as the local material coordinate system.

2.4 Material Variability Study

In order to assess the sensitivity of the whole bone response to variations in the mechanical properties, the material failure strength and strain were increased and decreased by one standard deviation (SD, shown in brackets in Table 2). Similarly, the elastic modulus was also increased and decreased by one standard deviation (SD shown in brackets in Table 1).

3. Results

3.1 Single Element Simulations for Constitutive Model Verification

Each of the three constitutive models was verified using single element simulations. The symmetric isotropic model (M_ISO_SYM) model was able to reproduce the complete tension stress-strain curve [Reilly and Burstein, 1975] (ultimate strain: 0.031 and ultimate stress: 0.135 GPa) (Appendix A). However, the lack of asymmetry in the model resulted in a compression curve comparable to the tension curve. Therefore, the literature stiffness and ultimate strength (17.28 GPa, 0.205 GPa) were under-predicted (16.4 GPa, 0.135 GPa) when the tension properties were used for compression simulations. The ultimate strain in compression (0.03) was similar to ultimate strain in tension, and was higher than the experimental ultimate compression strain of 0.0185 (Appendix A). The M_ISO_SYM constitutive model incorporated shear properties determined from the tension properties, resulting in the ultimate shear strength and strain values from the simulation being higher (0.08 GPa and 0.051) than the experimental values (0.05 GPa and 0.026) [Tang et al., 2015]. The model failed under shear loading when the effective plastic strain reached the failure limit, corresponding to a shear strain of 0.05, which over-predicted the experimental failure strain (0.026) [Tang et al., 2015].

The isotropic asymmetric (M_ISO_ASYM) model was able to reproduce the complete tension and compression stress-strain curves [Reilly and Burstein, 1975] (Appendix A). In tension, the model predicted the experimental ultimate stress and strain (0.135 GPa, 0.03). In compression, the stiffness and ultimate strength matched the literature data. However, the ultimate strain in compression (0.035) was higher than the experimental ultimate compression strain of 0.0185 (Appendix A), since failure was defined using the effective tensile plastic strain (0.0235). The shear strength was incorporated within the constitutive model and calculated using the compressive strength and a von Mises criterion, resulting in a higher ultimate shear strength (0.12 GPa) than the experimentally measured value (0.05 GPa) [Tang et al., 2015].

The orthotropic symmetric model (M_ORTHO_SYM) allowed for a definition of tension and shear properties in three directions, but did not include asymmetry in the elastic material properties. The longitudinal (1) direction was coincident with the osteon direction, and the model was able to reproduce the ultimate tensile strength (0.135 GPa). However, M_ORTHO_SYM under-predicted the ultimate tensile strain (0.0119) by approximately 60% due to the simplified damage definition, which did not allow for the damage peak to occur at both the ultimate tensile stress and strain experimental values (0.135 GPa, 0.031). The shear (0.05 GPa, 0.025) responses were predicted in agreement with the literature data. Early studies demonstrated that defining failure in compression and shear produced an unphysical response of the full femur model. Therefore, only failure in tension was defined for the M_ORTHO_SYM model. When damage was enabled (Table 2), material softening occurred prior to the

ultimate strength, in agreement with the experimental studies, and attributed to the formation of micro cracks [Ebacher et al., 2007].

3.2 Three-point Bending Force-Deflection and Fracture Response for Whole Femur Model

In the three-point bending simulation (Figure 4), the M_ISO_SYM model under-predicted the experimental bending failure force and displacement (4.29 kN and 16.7 mm) [Funk et al., 2004] by 17.4% (3.55 kN) and 31.2% (11.49 mm), respectively. The M_ISO_SYM model was outside the one standard deviation bounds for failure force (0.56 kN) and displacement (3.38 mm), and the maximum (4.94 kN, 23.3 mm) and minimum range (3.65 kN, 13 mm) for the test data. The M_ISO_SYM model predicted a localized fracture (Figure 5) at the location of the indenter (compression zone, bottom of bone), followed by transverse fracture propagation towards the tension region (top of the bone).

The M_ISO_ASYM model over-predicted the average experimental failure force by 5.8% (4.54 kN) and under-predicted the average failure displacement by 7.9% (15.39 mm). The failure force and displacement were within one standard deviation of the average. The M_ISO_ASYM model predicted a transverse fracture initiating on the compression side at the location of the impactor, due to contact stresses between the indenter (load point) and bone, before a fracture was observed on the tension side and propagated towards the mid-sagittal line of the femur into the compressive region.

The M_ORTHO_SYM model under-predicted the average experimental failure force and displacement by 6.4% (4.02 kN) and 22.1% (13.01 mm), respectively. The predicted failure force was within one standard deviation of the average, whereas the failure displacement was below the experimental minimum value. The M_ORTHO_SYM model predicted fracture initiation on the tension side of the bone, followed by propagation towards the mid-sagittal line of the femur into the compressive region, as reported in the literature. Although the fracture pattern did not bifurcate to form a butterfly fracture pattern commonly observed in experiments, the fracture initiated at the expected location (tension side) and formed a transverse fracture, as reported in the literature [Ebacher et. al, 2007; Kress et al., 1995; Rich, 2005].

Two aspects of material variability (material strength and strain at failure, and elastic moduli) were investigated with all three constitutive models in the three-point bending load case (Figure 6). All values were varied by one standard deviation relative to the average material properties. Varying the material strength had the largest effect on the M_ISO_ASYM model failure displacement, and the smallest effect on the M_ORTHO_SYM model. In contrast, varying the elastic modulus had the largest effect on the failure displacement of the M_ORTHO_SYM model. Varying material strength had a similar effect on the force at failure for all models, while varying modulus demonstrated only a modest effect. However, the fracture initiation location did not change for the models with variation in material properties (Figure 7). Importantly, the average experimental response remained within the range of model responses for the M_ORTHO_SYM model, including the material property variations, and the M_ORTHO_SYM model predicted the fracture initiation and fracture pattern in agreement with the experimental data.

3.3 Axial Torque-Rotation and Fracture Response for Whole Femur Model

In torsion, the original M_ISO_SYM and the M_ISO_ASYM models both over-predicted the experimental range of results (200% higher failure torque) whereas the M_ORTHO_SYM model fell within the experimental range.

The M_ISO_SYM material model (378.11 Nm) (Figure 8) over-predicted the average experimental failure torque of 183 Nm [Martens et al., 1980] by 107%, and exceeded the upper boundary of the test corridor failure torque (111 Nm to 286 Nm). Considering the rotation to failure, the M_ISO_SYM model (21.18 degrees) was 6% higher than the average experimental value (20.0 degrees). The M_ISO_SYM model (Figure 9) predicted fracture initiation in the vicinity of the lesser trochanter. The fracture propagated longitudinally through the diaphysis, and then transversely at a location past the mid-diaphysis and approximately one-third from the lesser trochanter, resulting in horizontal transverse fractures at these locations.

The asymmetric (M_ISO_ASYM) model (406.64 Nm) over-predicted the average experimental failure torque of 183 Nm by 122%, and exceeded both the upper boundary of the failure torque. The M_ISO_ASYM model rotation at failure (20.1 degrees) was in close agreement with the experimental average value of 20.0 degrees. The M_ISO_ASYM model predicted fracture initiation in the vicinity of the lesser trochanter, followed by longitudinal propagation, and finally a transverse fracture across the diaphysis.

The M_ORTHO_SYM model (245.40 Nm) over-predicted the average failure torque by 34%, but remained within one standard deviation of the average test data [Martens et al., 1980]. The M_ORTHO_SYM rotation at failure (16.8 degrees) under-predicted the average experimental value by 16%, but remained within one standard deviation of the average test data. The M_ORTHO_SYM model predicted fracture initiation at the mid-diaphysis, followed by longitudinal propagation across the diaphysis in the vicinity of the epiphyses.

The result of varying the material failure strength and strain, as well as of the elastic modulus for the torsional load cases were comparable to the outcomes of the bending case. An increase of the material failure strength and strain increased the rotational displacement at failure for all models, and was most pronounced in the M_ISO_SYM model (Figure 10). The failure moment also increased with an increase in material strength and strain values, and was most pronounced in the M_ORTHO_SYM model (Figure 10). On the other hand, increasing the elastic modulus value decreased the failure rotational displacement for all the models, with the most significant effect for the M_ORTHO_SYM model. The failure moment did not significantly change (less than 10%) due to variation of the elastic modulus. In general, the fracture initiation location did not change, except for the M_ISO_SYM model with -1SD in strength and strain reduced by one standard deviation (-1SD), where fracture occurred at the interface between the epiphyses and diaphysis (highlighted in a red box in Figure 11).

4. Discussion

4.1 Single Element Simulations

The results of the single element verification models were in good agreement with the experimental data (Appendix A), except for the shear strength for the M_ISO_SYM and M_ISO_ASYM models, due to the shear properties being determined from the tension properties. This is an important finding in terms of demonstrating that traditional metals models, using a von Mises yield surface, may not be appropriate for modeling cortical bone in shear or mixed-mode loading.

4.2 Three-Point Bending Test Simulations

In terms of kinetics, the M_ISO_ASYM model predicted the failure force closest to the experimental average (5.8% difference) and remained within one standard deviation of the average failure force. The total displacement at failure was lower than the average for the M_ORTHO_SYM and M_ISO_SYM models, with the M_ISO_ASYM model providing the closest values to the reported experimental data. This discrepancy was caused by potential contribution of the test apparatus and potting compliance to the overall measured deformation, which was not included in the model. This is an important consideration when comparing experimental and computational displacements, where the model displacement is often lower than the displacement reported in the experiment. Importantly, only the M_ORTHO_SYM model predicted fracture initiation on the tension side. Both the M_ISO_ASYM and M_ISO_SYM models incorrectly predicted fracture initiation on the compression side of the bone at the load point location, which is due to the use of a plastic strain failure criterion.

An additional study was undertaken to vary the three-point bending load velocity, and no difference in response or failure was identified, indicating that inertial effects were not significant in this case. In a second side study, the finite element mesh was refined by splitting the mesh twice (Appendix B). There was a slight reduction in failure load or moment as the mesh was refined; however, the model was generally consistent due to modest stress gradients at the failure location. Further, applying Richardson extrapolation demonstrated that the mesh was reasonably converged in terms of force and displacement at failure. However, the finer mesh typically produced a more distinct fracture pattern. It is acknowledged that a true convergence cannot be achieved when element erosion is present; however, for the practical purposes of this study, all three finite element mesh sizes provided similar results in bending (Appendix B).

4.3 Axial Torsion Test Simulations

The M_ORTHO_SYM model prediction of the moment at failure was the closest to the experimental average (34.1% difference), since the published material shear properties and strength were directly represented in the M_ORTHO_SYM constitutive model. The predicted rotation at failure was lower compared to the experimental average, but within one standard deviation of the average, attributed to potential compliance in the experimental test setup that was not included in the model. The M_ISO_SYM and M_ISO_ASYM models on the other hand over-predicted the moment at failure, as shear properties could not be defined in these constitutive models. As shown in the single element simulation results, the shear strength was determined from the material tensile or compressive strength using the von Mises failure criterion, leading to a maximum shear stress of approximately 0.115 GPa for the M_ISO_ASYM model and 0.076 GPa for the M_ISO_SYM model. Both values exceeded the published data by Tang et al. [2015], where the longitudinal ultimate shear strength was 0.029 GPa and the transverse shear strength was 0.050 GPa. In all cases, fracture initiated in the diaphysis of the bone and propagated longitudinally (Figure 9). None of the models predicted the typical spiral fracture pattern associated with axial torsion loading (Figure 9). Refining the finite element mesh, similar to the three-point bending case, provided similar failure moment and fracture pattern (Appendix B) indicating the mesh refinement was sufficient for this load case. Failure to predict the spiral fracture may be attributed to the element erosion definition based on a plastic strain criterion and requires further investigation.

4.4 Summary of Response

A summary of the constitutive model response for failure force and displacement to failure in three-point bending, and failure torque and corresponding rotation, are presented by normalizing each response to its respective average test value (Figure 12). It should be emphasized that the model utilized average mechanical properties from the literature measured at the material level, while the whole-bone simulation cases were compared to literature data on the three-point bending and axial torsion response. The response ranges (Figure 12) show the predicted model response for variations in material strength and strain to failure (+/- 1 standard deviation).

4.4 Model Limitations

Observable macro-scale fractures in bones initiate at stress concentrators, such as Haversian canals, or in the osteon and interstitial bone [Ebacher et al., 2007], and extend due to micro crack propagation mechanisms. Therefore, fracture studies in cortical bone have often been undertaken at the micro-structure scale [Ascenzi et al., 2013; Demirtas et al., 2016; Feerick et al., 2013; Ural et al., 2011]. In the current development of HBMs, however, incorporation of a detailed micro-model bone would incur a large computation cost and is therefore not feasible at present. Bone fracture has been simulated using the cohesive element or X-FEM approaches [Feerick et al., 2013; Ural et al., 2011; Demirtas et al., 2016; Ascenzi et al., 2013], and the present study utilized an element deletion approach to model failure, with initiation dependent on the maximum principal strain criterion. This method demonstrated the capacity to model fractures well at a whole-bone level [Schileo et al., 2008; Niebur et al., 2000]. The limitation of using the element deletion approach is a simultaneous crack initiation and propagation occur due to the lack of damage criterion, as the element is deleted when an elemental failure criterion is reached [Hambli et al., 2013; Hambli et al., 2012]. Therefore, the propagation direction is based on the deleted elements of the mesh. HBMs continue to utilize the element deletion approach; however, methods such as X-FEM may provide an important benefit in the future, despite their current high computational cost and instability issues in more complicated geometries.

One limitation of the current study is that strain rate effects were not incorporated in the constitutive models, because the experimental data [Funk, 2004; Kerrigan, 2003] did not indicate a statistically significant difference in failure forces between low and high rates of loading. Although strain rate effects have been reported for cortical bone, the literature is not in agreement in terms of the magnitude and presence of the effect. McElhaney [1966] reported that, in compression, higher strain rate resulted in higher stiffness, strength and modulus for embalmed human bone. A subsequent study by Crowninshield and Pope [1974] described similar results for bovine bones in tension. In contrast, Hansen et al. [2008] showed that rate effects did not result in higher failure strength or reduced ductility. This finding was explained, in part, by soaking of the bone in a saline-filled water bath, which was thought to delay the ductile to brittle bone transition. Burstein [1971] demonstrated that strain at failure can vary with the moisture content in bone, and the method used by McElhaney [1966] to adhere strain gauges on each specimen before testing may have induced drying of the bone [Crowninshield and Pope, 1974]. Differences in the literature results have also been attributed to different test methods and bones utilized in investigating rate effects [Hansen et al., 2008]. Furthermore, in a whole-bone three-point bending experiment conducted by Kerrigan et al. [2003], a single tibia was loaded quasi-statically (1 mm/s) and failed at a force of 3549 N. The average force to failure of the dynamic tibia tests was found to be 3578 N (SD 860 N, n=7), suggesting that the quasi-static and dynamic load conditions produced similar results, although only one quasi-static test was undertaken. It is well known that bone tissue exhibits viscoelastic properties [Asgharpour et al., 2014;

Hansen et al., 2008; Sanborn et al., 2016], and therefore this effect should be considered in future experimental and computational studies.

Existing metal plasticity models, as well as the models implemented in our study, are generally calibrated for tensile failure and therefore often predict tensile failure models in agreement with experimental data. Shear response is typically not predicted correctly by metal plasticity models due to the assumption of pressure independence in the yield surface, such as the von Mises yield surface. In this case, the shear strength is overestimated, as we have shown in the current study. Although anisotropic models address this challenge, the current models only approximate the expected spiral fracture pattern for torsional loading. Fracture is found to initiate in the shaft of the bone and subsequently progresses along the length of the bone, since this is the lowest strength plane available for the fracture (element erosion) to propagate.

One important aspect not addressed in this study was the use of average published cortical bone material properties (average age of 53, range 20 to 86), while the whole-bone tests were from PMHS with an average age of 59 (range 40 to 70). The mechanical properties and strengths were not adjusted for age or other factors, such as bone mineral density, known to affect bone strength. However, varying the strength and modulus properties in the model by one standard deviation from the average was found to account for some of the differences between the model predictions and the experimental results.

5. Conclusions

Assessment of constitutive models and properties requires an independent set of data with known boundary conditions and appropriate response metrics. This was achieved in the current study using whole femur three-point bending (force, displacement) and axial torsion (moment, rotation) experimental data, compared to a computational femur model from a current HBM and using published cortical bone material properties. In addition to kinetics and kinematics, failure was assessed using the ultimate load, failure initiation location and resulting fracture pattern, providing additional insight into model performance. Single element simulations were beneficial to verify the material model implementation while identifying fundamental limitations such as the over prediction of shear strength when using a von Mises yield surface assumption.

Existing isotropic metal plasticity models using cortical bone tensile properties predicted kinetics and kinematics in agreement with three-point bending experimental data, but incorrectly predicted bone failure to initiate at the point of load application and significantly over predicted the failure moment for axial torsion. In simplified constitutive models, it is recommended to use tensile properties since the tensile strength is associated with failure in three-point bending and axial torsion.

Considering material asymmetry modestly improved prediction of the three-point bending kinetics and kinematics but resulted in unphysical predicted failure initiation of the bone at the point of load application associated with the use of a plastic strain failure criterion. Similar to the symmetric isotropic model, using a von Mises yield surface assumption to estimate shear properties significantly over predicted the failure moment in axial torsion.

An orthotropic material model provided the best overall performance in terms of predicting the ultimate load in three-point bending (6.4% difference), maximum torque in axial torsion (34.1%

difference), the failure initiation location and fracture pattern in three-point bending, and the fracture initiation location for axial torsion. None of the models predicted a spiral fracture pattern for axial torsion and this should be investigated further. It was noted that the displacements to failure predicted by the computational models were typically lower than the experimentally measured displacements. Although varying the material properties within measured ranges explained some of this variability, it was noted that the finite element models used idealized boundary conditions with lower compliance compared to the experimental fixtures and this could explain the lower predicted displacement to failure values.

Average cortical bone material properties incorporated in an orthotropic material model provided good predictions of whole bone response and failure. Varying the material mechanical properties within one standard deviation provided results within the range of variability of the experimental whole-bone test data and therefore was able to explain some of the variability in the test data. The proposed cortical bone material properties implemented in an orthotropic constitutive model presents a significant improvement over the current modeling approaches in HBM.

Acknowledgements:

The authors would like to thank Honda R&D Americas for financial support, the Global Human Body Models Consortium for providing the femur model, and Compute Canada for providing the necessary computing resources.

Appendix A: Material Model Responses in Single Element Simulations

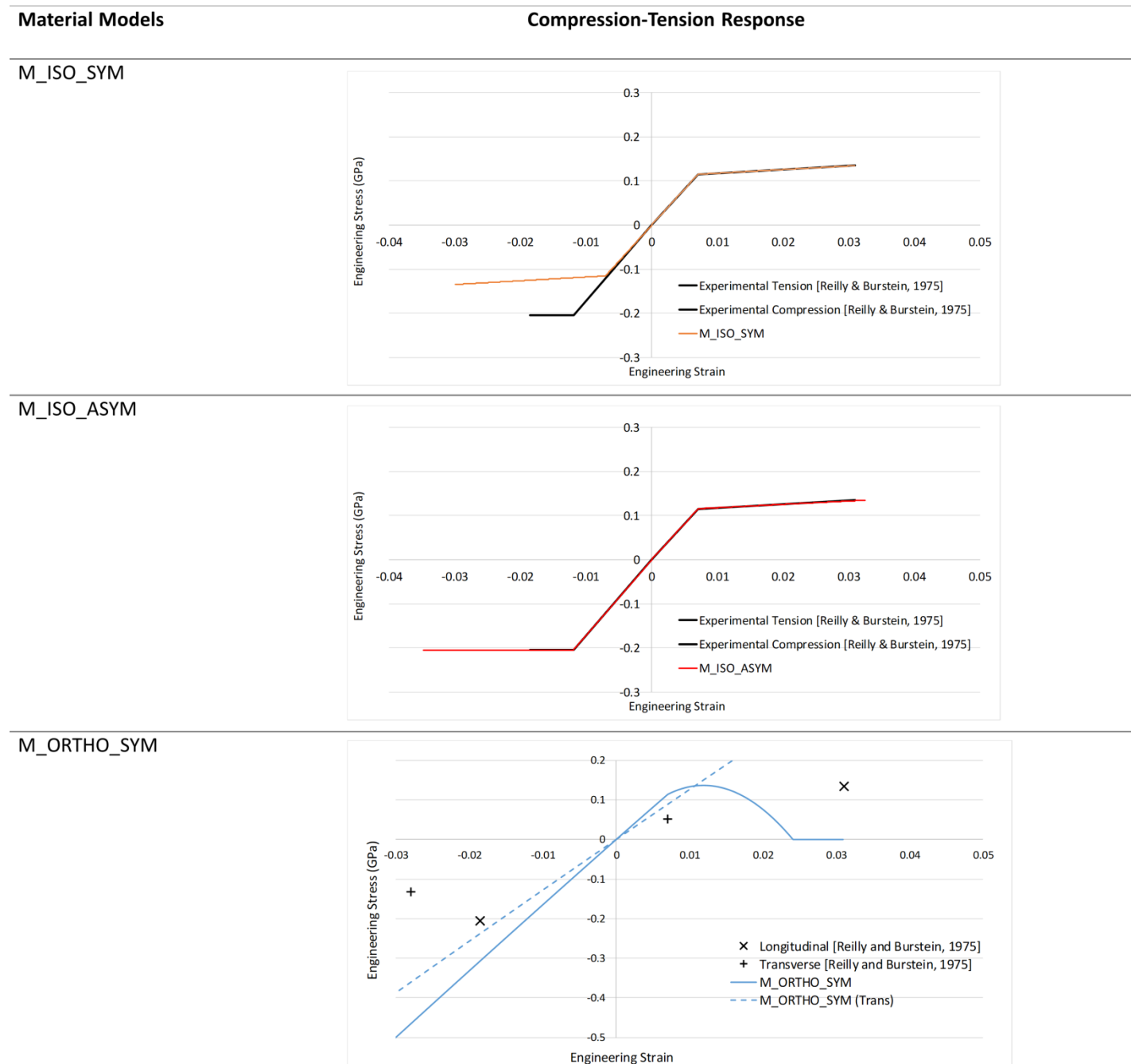
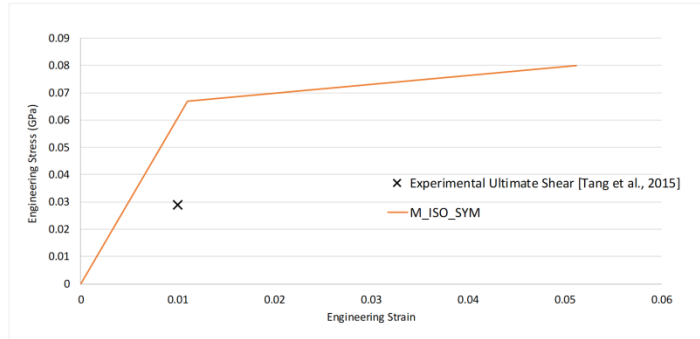


Figure A.1: Comparison of Compression-Tension Responses in Single Element Simulations for M_ISO_SYM, M_ISO_ASYM, and M_ORTHO_SYM Models.

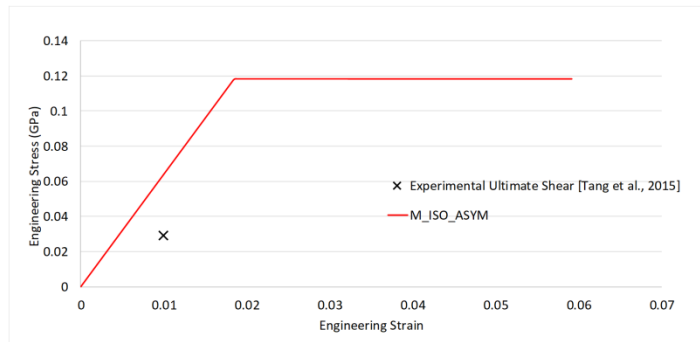
Material Models

Shear Response

M_ISO_SYM



M_ISO_ASYM



M_ORTHO_SYM

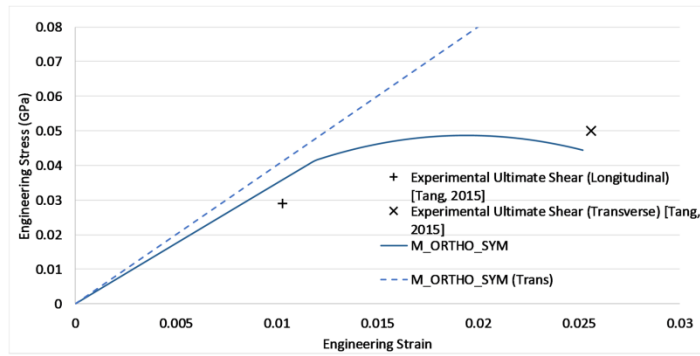


Figure A.2: Comparison of Shear Responses in Single Element Simulations for M_ISO_SYM, M_ISO_ASYM, and M_ORTHO_SYM Models.

Appendix B: Mesh Refinement Analysis

A mesh refinement analysis was performed by splitting the elements once (1 element into 4 elements) and then twice (1 element into 16 elements). In the bending model, the original mesh with the indenter has 40,496 elements with an element size of 3 mm, the medium mesh (single split) has 260,768 elements with an element size of 1.5 mm, and the fine mesh (double split) has 1,999,600 elements with an element size of 0.75 mm. In the torsion model, the original model has 34,496 elements with an element size of 3 mm, the medium mesh (single split) has 254,768 elements with an element size of 1.5 mm and the fine mesh (double split) has 1,956,800 elements with an element size of 0.75 mm.

The analysis demonstrated that the response was consistent for three mesh sizes throughout the loading phase. There was a slight reduction in failure load or moment as the mesh was refined; however, the model was generally consistent due to modest stress gradients at the failure location. Further, applying Richardson extrapolation demonstrated that the mesh was reasonably converged in terms of force and displacement at failure. However, the finer mesh typically produced a more distinct fracture pattern. It is acknowledged that a true convergence cannot be achieved when element erosion is present; however, for the practical purposes of this study, all three finite element mesh sizes provided similar results in bending (Figure B.1 and Figure B.2) and torsion (Figure B.3 and Figure B.4).

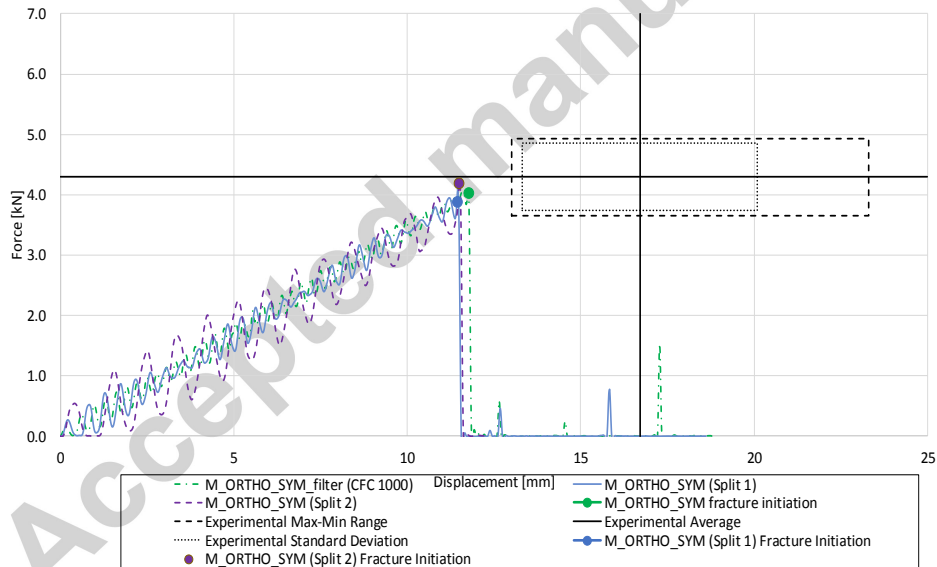


Figure B.1: Force-time history for the femur bending case and three mesh resolutions.

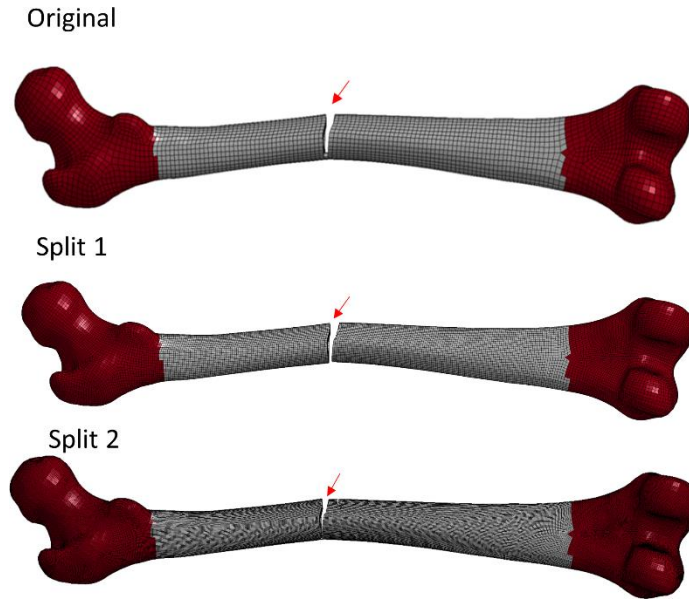


Figure B.2: Fracture pattern for the femur bending case and three mesh resolutions.

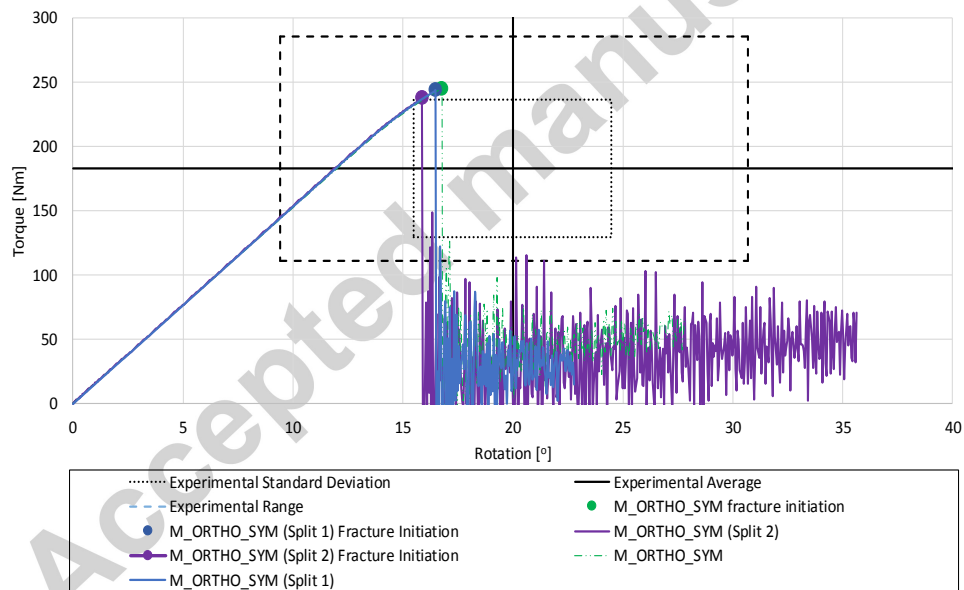


Figure B.3: Force-time history for the femur torsion case and three mesh resolutions.

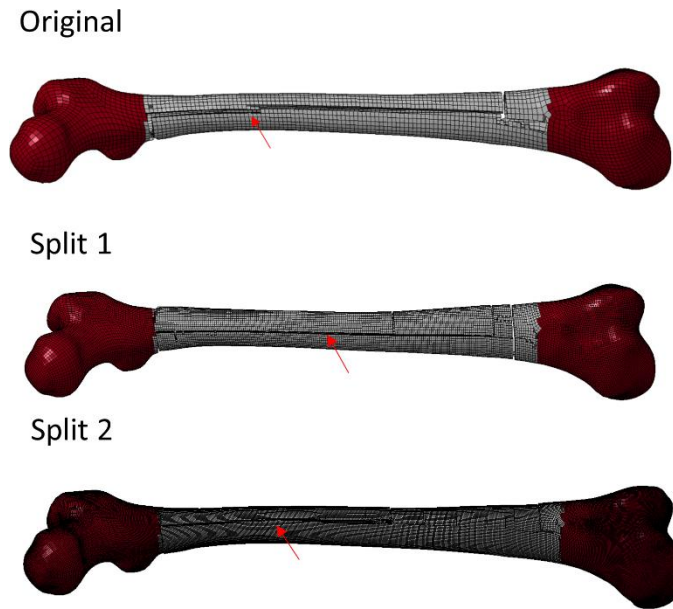


Figure B.4: Fracture pattern for the femur torsion case and three mesh resolutions.

References

- Abdel-Wahab, A.A., Maligno, A.R., Silberschmidt, V.V. (2012). Micro-scale modelling of bovine cortical bone fracture: Analysis of crack propagation and microstructure using X-FEM. *Computational Materials Science* 52, 128–135.
- Abbreviated Injury Scale (2005) Association for the Advancement of Automotive Medicine. Chicago, Illinois.
- Ali, A.A., Cristofolini, L., Schileo, E., Hu, H., Taddei, F., Kim, R.H., Rullkoetter, P.J., Laz, P.J. (2014). Specimen-specific modeling of hip fracture pattern and repair. *Journal of Biomechanics* 47, 536–543.
- Ascenzi, M., Kawas, N.P., Lutz, A., Kardas, D., Nackenhorst, U., Keyak, J.H. (2013). Individual-specific multi-scale finite element simulation of cortical bone of human proximal femur. *Journal of Computational Physics* 244, 298–311.
- Asgharpour, Z., Zioupos, P., Graw, M., Peldschus, S. (2014). Failure modelling of trabecular bone using a non-linear combined damage and fracture voxel finite element approach. *Forensic Science International* 236, 109–116.
- Ashman, R.B., Cowin, S.C., Van Buskirk, W.C., Rice, J.C. (1984). A continuous wave technique for the measurement of the elastic properties of cortical bone. *Journal of Biomechanics* 17 (5), 349–361.
- Burstein, A.H., Frankel, V.H. (1971). A standard test for laboratory animal bone. *Journal of Biomechanics* 4 (2), 155–158.

- Carter, D.R., Spengler, D.M. (1982). Biomechanics of fracture. *Bone in clinical orthopaedics*, 305–334. WB Saunder, Philadelphia, PA.
- Cowin, S.C. (2001). *Bone mechanics handbook*, CRC Press. Boca Raton, FL.
- Crowninshield, R.D., Pope, M.H. (1974). The Response of Compact Bone in Tension at Various Strain Rates. *Annals of Biomedical Engineering* 2, 217–225.
- Currey, J.D. (2002). *Bones: Structure and mechanics*. Princeton University Press, Princeton, NJ.
- Demirtas, A., Curran, E., Ural, A. (2016). Assessment of the effect of reduced compositional heterogeneity on fracture resistance of human cortical bone using finite element modeling. *Bone* 91, 92–101.
- DeWit, J.A., Cronin, D.S (2012). Cervical Spine Segment Finite Element Model for Traumatic Injury Prediction. *Journal of the Mechanical Behavior of Biomedical Materials* 10, 138–150, DOI: 10.1016/j.jmbbm.2012.02.015.
- Ebacher, V., Tang, C., McKay, H., Oxland, T.R., Guy, P., Wang, R. (2007). Strain redistribution and cracking behavior of human bone during bending. *Bone* 40, 1265–1275.
- Feerick, E.M., Liu, X., McGarry, P. (2013). Anisotropic mode-dependent damage of cortical bone using the extended finite element method (XFEM). *Journal of the Mechanical Behavior of Biomedical Materials* 20, 77–89.
- Fondrk, M., Bahniuk, E., Davy, D. (1999). A Damage Model for Nonlinear Tensile Behavior of Cortical Bone. *Journal of Biomechanical Engineering*, 533–541.
- Fondrk, M., Bahniuk, E., Davy, D. (1999). Inelastic strain accumulation in cortical bone during rapid transient tensile loading. *Journal of Biomechanical Engineering*, 616–621.
- Funk, J.R., Kerrigan, J.R., Crandall, J.R. (2004). Dynamic bending tolerance and elastic-plastic material properties of the human femur. In *Annual Proceedings/Association for the Advancement of Automotive Medicine* 48, 215-233. Association for the Advancement of Automotive Medicine, Chicago, IL.
- Garcia, D., Zysset, P., Curnier, M. (2010). A 1D elastic plastic damage constitutive law for bone tissue. *Archive of Applied Mechanics*, 543–555.
- Garcia, D., Zysset, P., Charlebois, M., Curnier, A. (2009). A three-dimensional elastic plastic damage constitutive law for bone tissue. *Biomechanics and Modeling in Mechanobiology*, 149–165.
- Giambini, H., Qin, X., Dragomir-Daescu, D., An, K., Nassr, A. (2016). Specimen-specific vertebral fracture modeling: a feasibility study using the extended finite element method. *Medical & Biological Engineering & Computing*, 54 (4), 583–593.
- Gibson, L.J., Ashby, M.F. (1988). *Cellular Solids: structure and properties*. Pergamon Press. Oxford. England.
- Gierczycka, D., Watson, B., Cronin D.S. (2015). Investigation of Occupant Arm Position and Door Properties on Thorax Kinematics in Side Impact Crash Scenarios, Comparison of ATD and Human Models. *International Journal of Crashworthiness* 20 (3), 242–269 DOI: 10.1080/13588265.2014.998000.

- Hambli, R., Bettamer, A., Allaoui, S. (2012). Finite element prediction of proximal femur fracture pattern based on orthotropic behaviour law coupled to quasi-brittle damage. *Medical Engineering & Physics* 34, 202–210.
- Hambli, R., Thurner, P.J. (2013). Finite element prediction with experimental validation of damage distribution in single trabeculae during three-point bending tests. *Journal of the Mechanical Behavior of Biomedical Materials* 27, 94–106.
- Hansen, U., Zioupos, P., Simpson, R., Currey, J.D., Hynd, D. (2008). The effect of strain rate on the mechanical properties of human cortical bone. *Journal of Biomechanical Engineering* 130 (1), 1-8.
- Harrison, N.M., McDonnell, P., Mullins, L., Wilson, N., O'Mahoney, D., McHugh, P. (2013). Failure modelling of trabecular bone using a non-linear combined damage and fracture voxel finite element approach. *Biomech Model Mechanobiol* 12, 225–241.
- Idkaidek, A. and Jasiuk, I. (2016). Cortical bone fracture analysis using XFEM-case study. *International Journal for Numerical Methods in Biomedical Engineering*; DOI: 10.1002/cnm.2809.
- Iwamoto, M., Mik, i K., Tanaka, E. (2005). Ankle Skeletal Injury Predictions Using Anisotropic Inelastic Constitutive Model of Cortical Bone Taking into Account Damage Evolution. *Stapp Car Crash Journal* 49, 133–156.
- Kennedy, E.A., Hurs,t W.J., Stitzel, J.D., Cormier, J.M., Hansen, G.A., Smith, E.P., Duma, S.M. (2004). Lateral and Posterior Dynamic Bending of the Mid-Shaft Femur: Fracture Risk Curves for the Adult Population, *Stapp Car Crash Journal* 48, 1-25.
- Kerrigan, J.R., Bhalla, K.S., Madeley, N.J., Funk, J.R., Bose, D., Crandall, J.R. (2003). *Experiments for establishing pedestrian-impact lower limb injury criteria*. SAE Technical Paper No. 2003-01-0895.
- Khor, F., Watson, B., Gierczycka, D., Malcolm, S., Panzer, M.B., Cronin, D.S. (2016a). Effect of Cortical Bone Material Asymmetry Using a 3-Point Bend Test Simulation. In *Proceedings of the International Research Council on Biomechanics of Injury Conference*, IRCOBI Asia, Seoul, South Korea.
- Khor, F., Cronin, D. (2016b). Constitutive Modeling of Cortical and Trabecular Bone Applied to Compression Loading and Failure of a Lower Cervical Spine Segment Model. In *Proceedings of the Injury Biomechanics Symposium*, Ohio State University, Columbus, OH.
- Kress, T.A., Porta, D.J., Snider, J.N., Fuller, P.M., Psihogios, J.P., Heck, W.L., Frick, S.J., Wasserman, J.F. (1993). Human femur response to impact loading. In *Proceedings of the International Research Council on the Biomechanics of Injury Conference* (Vol. 21, pp. 93–104). IRCOBI, Eindhoven, the Netherlands.
- Kress, T.A., Porta, D.J., Snider, J.N., Fuller, P.M., Psihogios, J.P., Heck, W.L., Frick, S.J., Wasserman, J.F. (1995). Fracture patterns of human cadaver long bones. In *Proceedings of the International Research Council on the Biomechanics of Injury Conference* (Vol. 23, pp. 155–169). IRCOBI, Brunnen, Switzerland.
- Li, S., Abdel-Wahab, A.A., Silberschmidt, V.V. (2013). Analysis of fracture processes in cortical bone tissue. *Engineering Fracture Mechanics* 110, 448–458.
- LSTC (2016). *LS-DYNA Keyword User's Manual*. Livermore, CA.
- LSTC (2016). *LS-DYNA Theory Manual*. Livermore, CA.

- Martens, M., Van Audekercke, R., De Meester, P., Mulier, J.C. (1980). The Mechanical Characteristics of the Long Bones of the Lower Extremity in Torsional Loading. *Journal of Biomechanics* 13, 667–676.
- Martin, R.B., Burr, D.B., Sharkey, N.A. (1998). *Skeletal tissue mechanics*. Springer.
- Mather, B.S. (1967). Correlations Between Strength and Other Properties of Long Bones. *The Journal of Trauma* 7 (5).
- McElhaney, J.H. (1966). Dynamic response of bone and muscle tissue. *Journal of Applied Physiology* 21 (4), 1231–1236.
- Mischinski, S., Ural, A. (2011). Finite Element Modeling of Microcrack Growth in Cortical Bone. *Journal of Applied Mechanics* 78.
- Niebur, G.L., Feldstein, M.J., Yuen, J.C., Chen, T.J., Keaveny, T.M. (2000). High-resolution finite element models with tissue strength asymmetry accurately predict failure of trabecular bone. *Journal of Biomechanics* 33, 1575-1583.
- Porta, D., Frick, S., Kress, T., Fuller, P. (1997). Production of spiral fractures in human cadaver long bones by use of a simple torsion machine. *Biomedical Sciences Instrumentation* 33, 418–422.
- Reilly, D.T., Burstein, A.H. (1975). The elastic and ultimate properties of compact bone tissue. *Journal of Biomechanics* 8 (6), 393–405.
- Reilly, D.T., Burstein, A.H., Frankel, V.H. (1974). The elastic modulus for bone. *Journal of Biomechanics* 7, 271–275.
- Rich, J., Dean, D.E., Powers, E., Robert, H. (2005). *Forensic medicine of the lower extremity: human identification and trauma analysis of the thigh, leg and foot*. Ed. Totawa, N.J, Humana Press.
- Sanborn, B., Gunnarsson C.A., Foster, M., Weerasooriya, T. (2016). Quantitative Visualization of Human Cortical Bone Mechanical Response: Studies on the Anisotropic Compressive Response and Fracture Behavior as a Function of Loading Rate. *Experimental Mechanics*, 56:81-95, DOI 10.1007/s11340-015-0060-y.
- Schileo, E., Taddei, F., Cristofolini, L., Viceconti, M. (2008). Subject-specific finite element models implementing a maximum principal strain criterion are able to estimate failure risk and fracture location on human femurs tested in vitro. *Journal of Biomechanics*, 41, 356–367.
- Schmitt, K-U., Niederer, P.F., Cronin, D.S., Muser, M.H., Walz, F. (2014). *Trauma Biomechanics: An Introduction to Injury Biomechanics*. Springer-Verlag, Berlin Heidelberg.
- Sharir, A., Barak, M.M., Shahar, R. (2008). Whole bone mechanics and mechanical testing. *The Veterinary Journal*, 177 (1), 8–17.
- Tanaka, M., Wada, S., Nakamura, M. (2012). *Computational Biomechanics: Theoretical Background and Biological/Biomedical Problems*. Osaka: Springer.
- Tang, T., Ebacher, V., Crompton, P., Guy, P., McKay, H., Wang, R. (2015). Shear deformation and fracture of human cortical bone. *Bone* 71, 25–35.

Tscherne, H., Oestern, H.J. (1982). A new classification of soft-tissue damage in open and closed fractures. *Unfallheilkunde*, 85(3), 111–115.

Turner, C.H. (2006). Bone strength: current concepts. *Annals of the New York Academy of Sciences* 1068 (1), 429–446.

Untaroiu, C.D., Yue, N., Shin, J. (2013). *A Finite Element Model of the Lower Limb for Simulating Automotive Impacts*, 41(3), 513–526.

Ural, A., Zioupos, P., Buchanan, D., Vashishth, D. (2011). The effect of strain rate on fracture toughness of human cortical bone: A finite element study. *Journal of the Mechanical Behavior of Biomedical Materials* 4, 1021–1032.

Zysset, P.K, Dall'Ara, E., Varga, P., Pahr, D.H. (2013). Finite element analysis for prediction of bone strength. *BoneKEy Reports* 2, Article number: 386, DOI:10.1038/bonekey.2013.120.

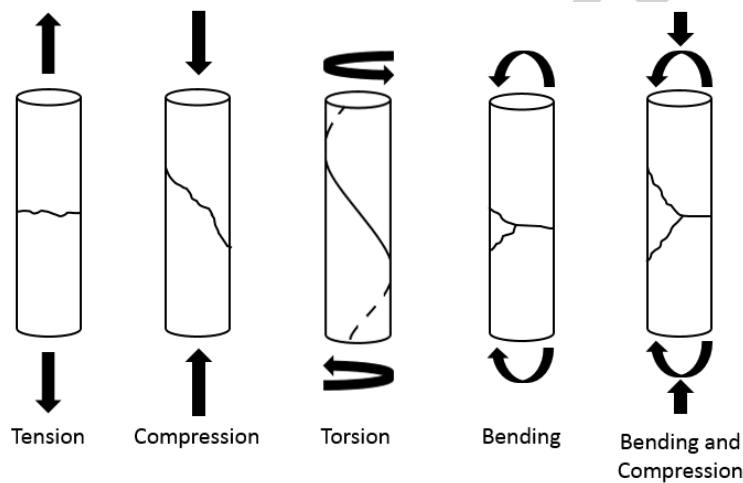


Figure 1: Typical Fracture Patterns by Types of Loading. [Redrawn from Carter & Spengler, 1982]

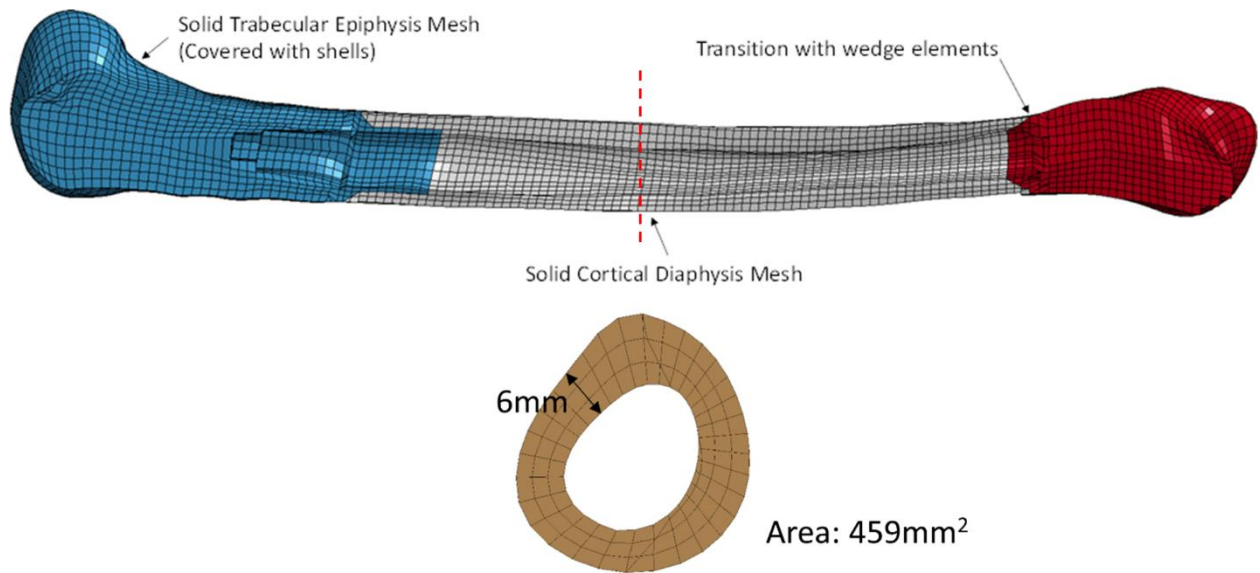


Figure 2: HBM femur extracted from the full body model with the solid elements shown and the cross-sectional area thickness and area calculation from the femur mid-shaft

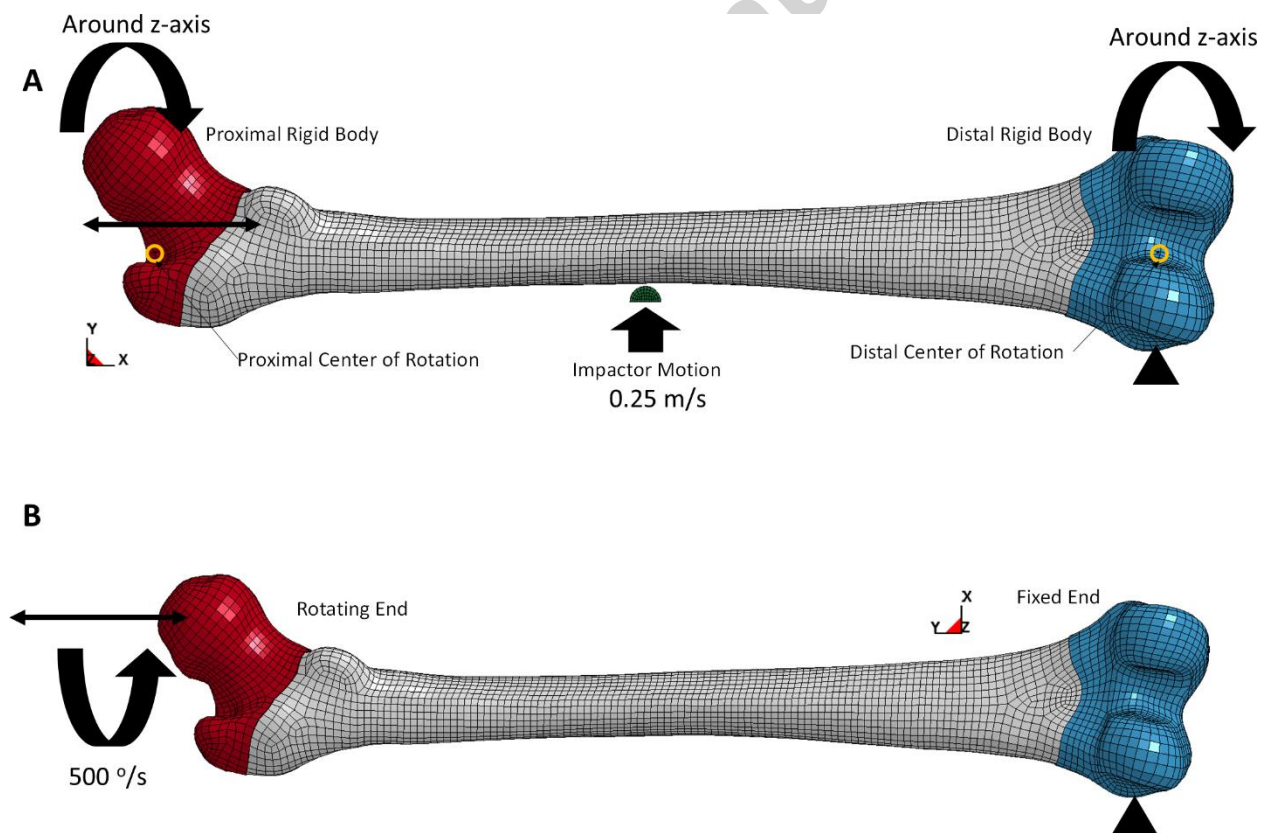


Figure 3: Boundary Condition Set Up in A) Bending (Medio-Lateral Direction) and B) Axial Torsion.

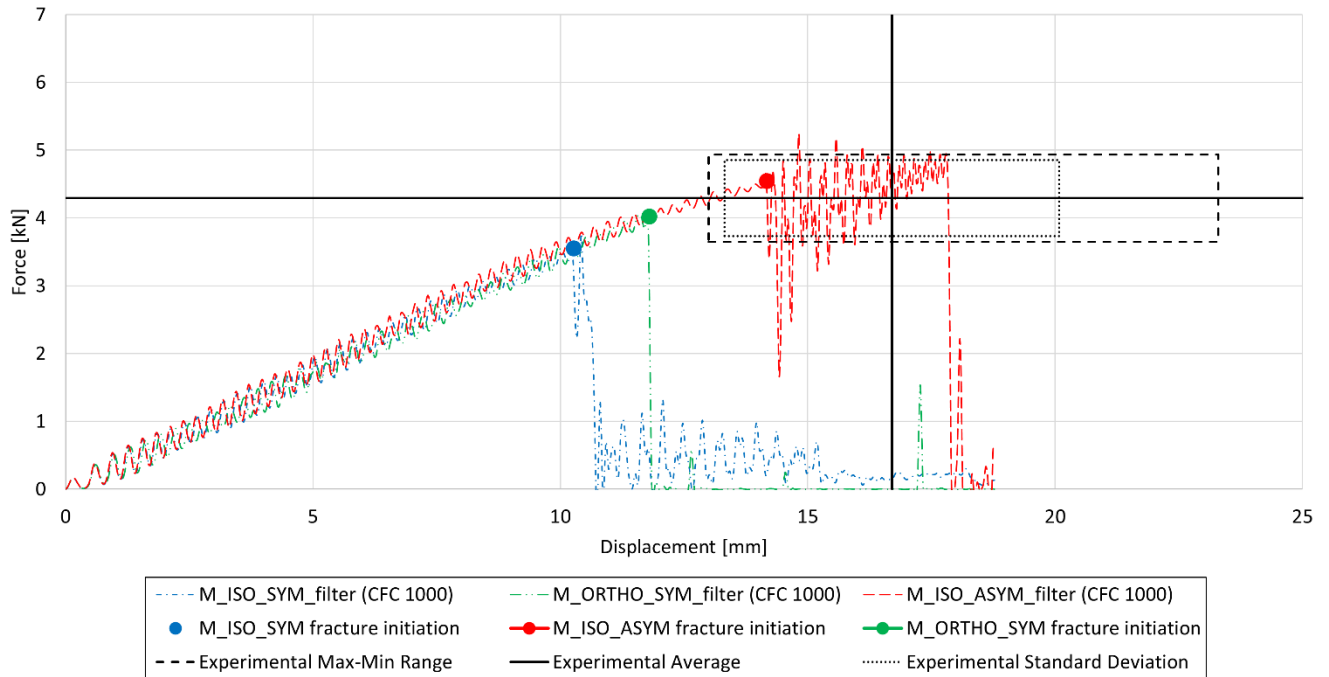


Figure 4: Force-displacement response in bending (average experimental response from Funk et al. [2004] shown as solid black lines, experimental max-min range shown with dashed black lines, experimental standard deviation range shown with dotted black lines).

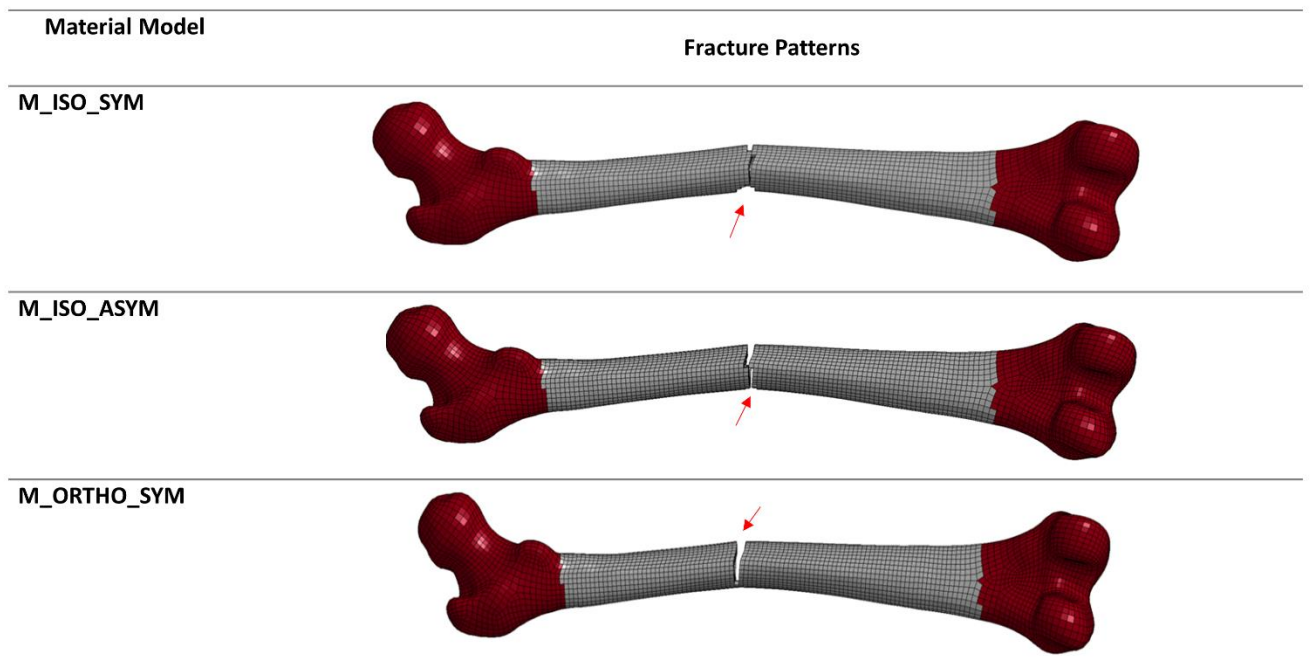


Figure 5: Predicted fracture patterns for three-point bending (arrow identifies fracture initiation).

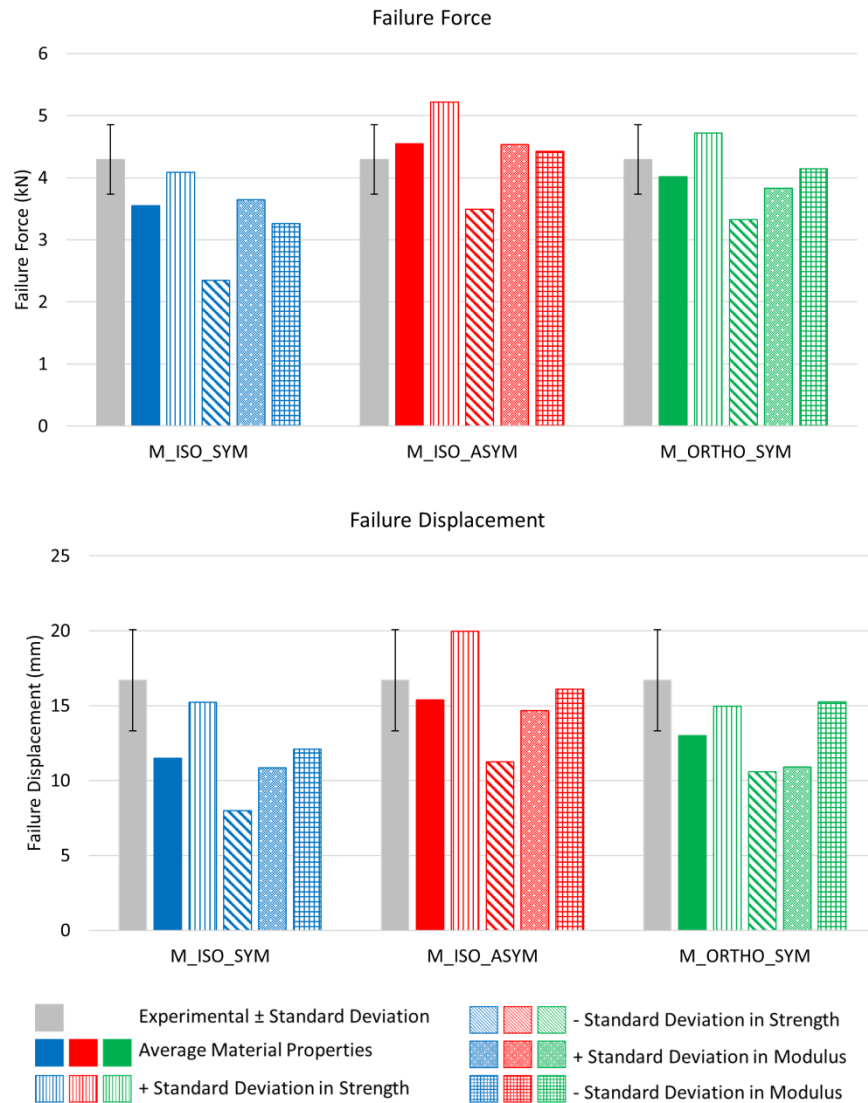


Figure 6: Three-point bending force (top) and displacement (bottom) at failure, varying material strength and modulus by one standard deviation.

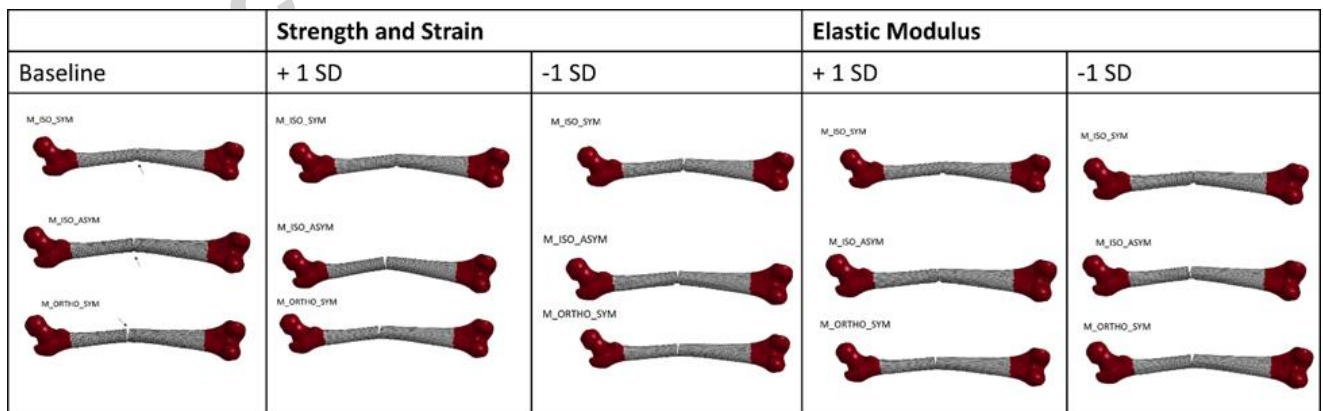


Figure 7: Fracture patterns for the three investigated constitutive models and variations of the material properties in bending.

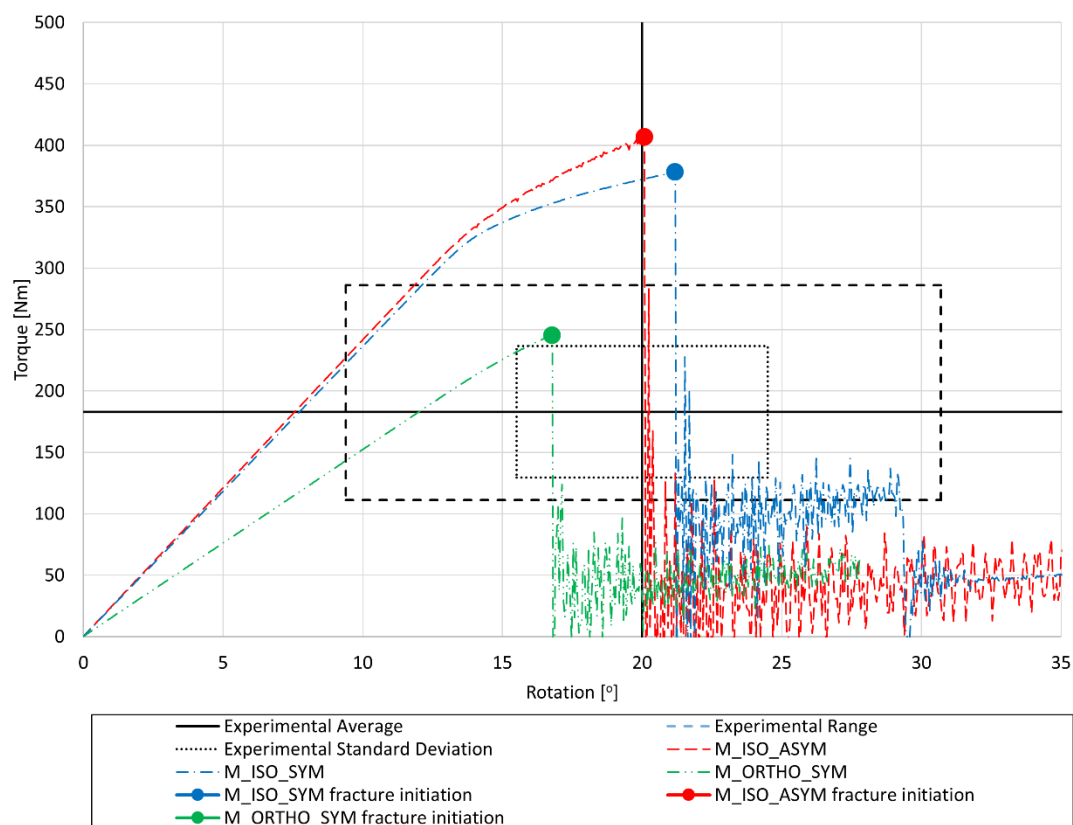


Figure 8: Torque-rotation response (average test response from Martens et al. [1980] shown as solid black lines, experimental max-min range is shown with dashed black lines, experimental standard deviation range is shown with dotted black lines).

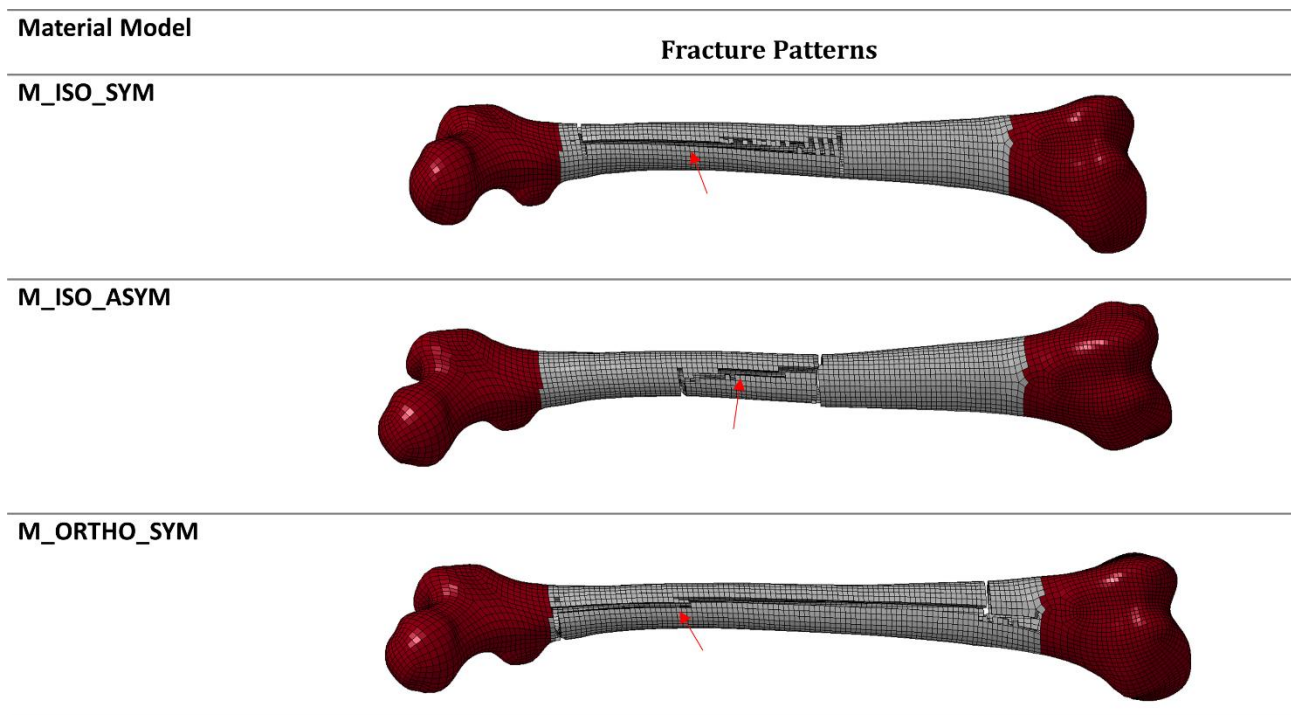


Figure 9: Predicted fracture patterns for axial torsion (arrow identifies fracture initiation).

Accepted manuscript

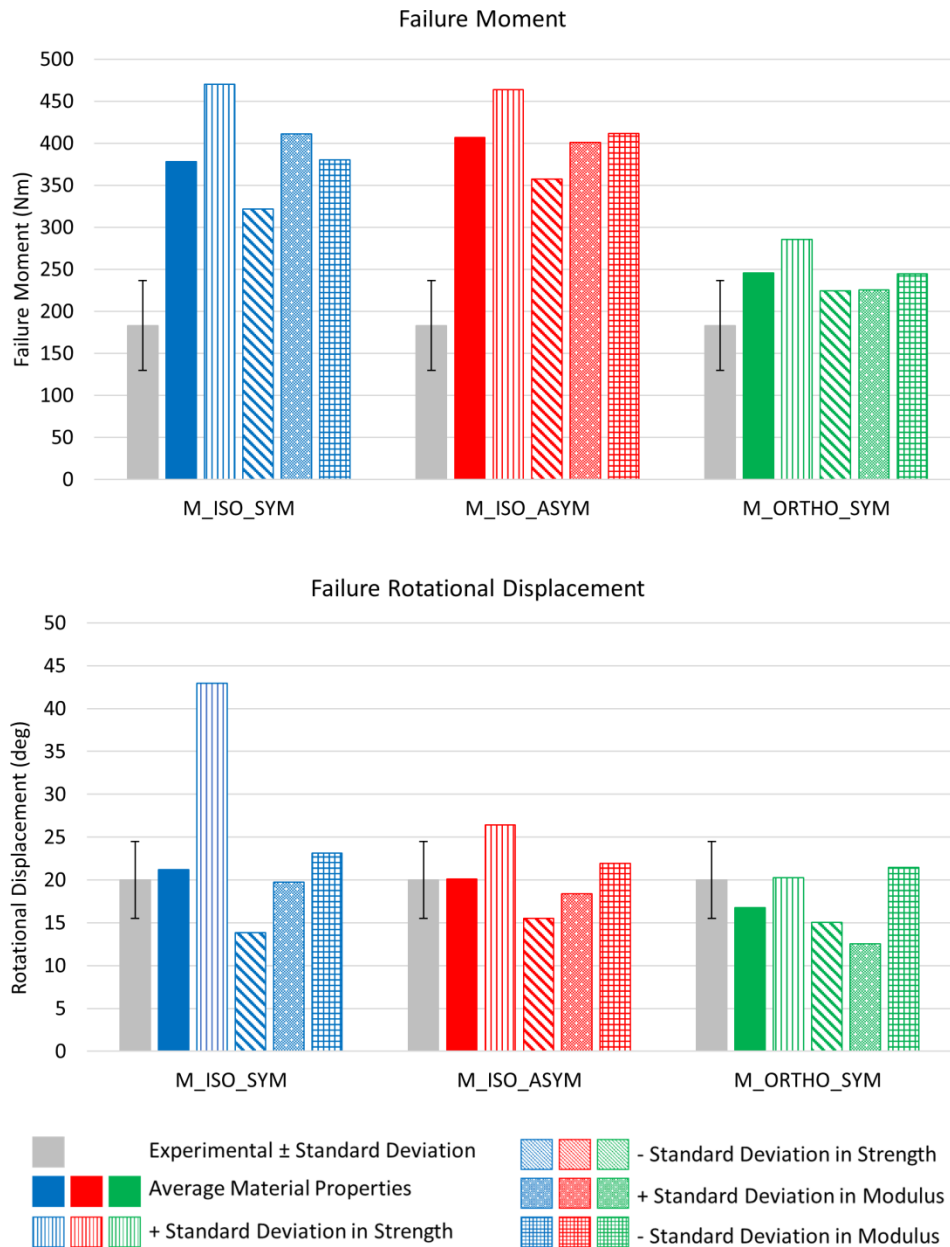


Figure 10: Axial torsion torque (top) and rotation (bottom) at failure, varying material strength and modulus by one standard deviation.

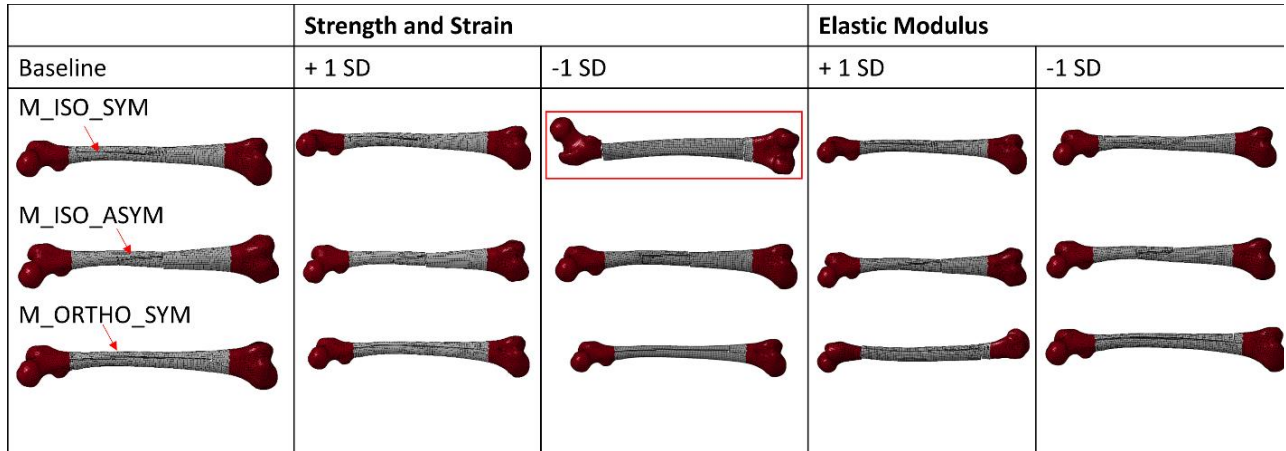


Figure 11: Fracture patterns for the three investigated constitutive models and variations of the material properties in torsion.

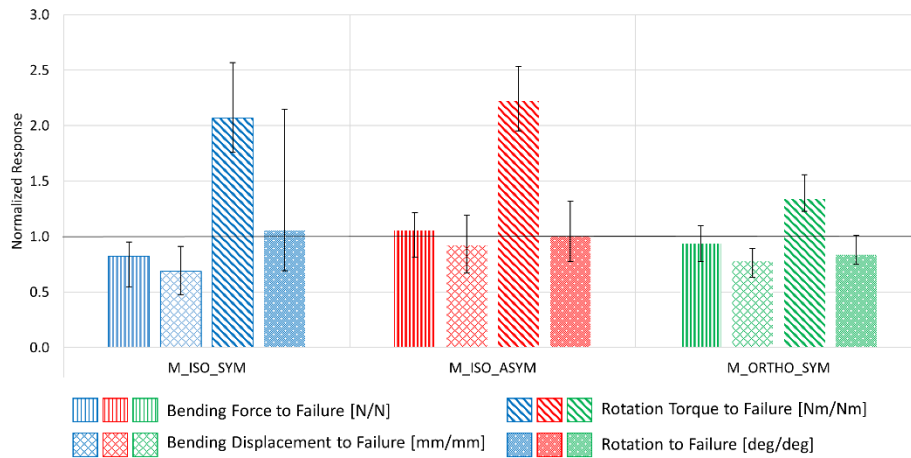


Figure 12: Summary of normalized model response (horizontal line represents normalized average experimental response; error bars correspond to +/- one standard deviation in material strength for the simulations).

Table 1: Summary of cortical bone elastic properties for both tension-based and compression-based models

	GHBMCM50 HBM	Tension	Compression
Longitudinal Young's modulus (Osteon direction) (E1), GPa (SD)	13.5	16.4 (2.11) [Reilly and Burstein, 1974]	17.28 (1.56) [Reilly and Burstein, 1974]
Transverse Young's modulus (E2=E3), GPa (SD)	N/A	12.7 (2.99) [Reilly and Burstein, 1975]	11.7 (10.1)[Reilly and Burstein, 1975]
Shear Modulus (G23=g32), GPa (SD)	N/A	4.0 (0.4) [Tang et al., 2015]	4.0 (0.4) [Tang et al., 2015]
Shear Modulus (G13=G12=G32=G21), GPa (SD)	N/A	3.5 (0.8)[Tang et al., 2015]	3.5 (0.8) [Tang et al., 2015]
Bulk Modulus (K), GPa	NA	10.31	10.87
Poisson's ratio (v21=v31)	0.3	0.235 [Ashman et al., 1984]	0.235 [Ashman et al., 1984]
Poisson's ratio (v32)	N/A	0.376 [Ashman et al., 1984]	0.376 [Ashman et al., 1984]

Table 2: Summary of cortical bone material strength properties

	GHBMC M50			
	HBM	Tension	Compression	Shear
Longitudinal (Osteon) direction				
Ultimate strength (GPa) (SD)	0.134	0.135 (0.016) [Reilly and Burstein, 1975]	0.205 (0.017) [Reilly and Burstein, 1975]	0.029 (0.006) [Tang et al., 2015]
Failure strain (-) (SD)	0.0218	0.031 (0.007) [Reilly and Burstein, 1975]	0.0185 (0.003) [Reilly and Burstein, 1975]	0.010 [Tang et al., 2015]
Transverse direction				
Ultimate stress (GPa) (SD)	N/A	0.053 (0.0107) [Reilly and Burstein, 1975]	0.131 (0.0207) [Reilly and Burstein, 1975]	0.050 (0.006) [Tang et al., 2015]
Ultimate strain (SD)	N/A	0.007 (0.0014) [Reilly and Burstein, 1975]	0.028 (0.0029) [Reilly and Burstein, 1975]	0.026 [Tang et al., 2015]
Damage Parameter				
Longitudinal (Osteon) direction				
D	-	1.4	-	0.494

Table 3: Description and summary of material models in this study

LS-DYNA Material Model [LSTC, 2016]		Description	Material Properties (Tables 2 and 3)	Constitutive Model comparison	Model Single Element Verification Properties
Case 1. M_ISO_SYM	MAT_019: MAT_STRAIN_RATE_DEPENDENT_PLASTICITY	Isotropic, symmetric in tension and compression, metals plasticity model	Tension properties	Symmetric, isotropic tension-based properties	Symmetric, isotropic tension-based properties
Case 2. M_ISO_ASYM	MAT_124: MAT_PLASTICITY_COMPRESSION_TENSION	Isotropic, tension-compression asymmetry, metals plasticity model	Tension and compression properties	Asymmetric, isotropic tension-based properties	Symmetric, isotropic tension-based properties
Case 3. M_ORTHO_SYM	MAT_221: MAT_ORTHOTROPIC_SIMPLIFIED_DAMAGE	Anisotropic, symmetric, damage-based failure model	Tension properties	Symmetric, orthotropic properties	Symmetric, isotropic tension-based properties

Table 4: Whole-bone femur tests for model validation

		3 Point Bending	Axial Torsion
Study		Funk et al. 2004	Martens et al. 1980
Number of Samples		7	47
Failure Force \ Torque	Average (SD)	4294 N (0.56)	183 Nm (53.52)
	Maximum	4943 N	286 Nm
	Minimum	3646 N	111 Nm
Failure Displacement \ Rotation	Average (SD)	16.7 mm (3.38)	20.0 ° (4.49)
	Maximum	23.3 mm	30.7 °
	Minimum	13.0 mm	9.4 °

Table 5: Anthropometric data of the PMHS bone donors (Funk et al. 2004)

Specimen #	Gender	Age (years)	Average femur length (mm)	Area (mm ²)
1	M	67	481	464
2	M	59	476	501
3	M	40	486	449
4	M	55	477	411
5	M	70	445	448
6	M	69	467	469
7	M	51	499	576
8	M	66	446	459
Average (SD)		59.6 (10.5)	472.1 (18.8)	472.1 (48.9)

Highlights:

- Cortical bone material properties were assessed using a human femur FE model and whole bone experiments.
- Material asymmetry and anisotropy were evaluated using three-point bending and torsional load cases.
- Variations in material properties accounted for some difference between the model and experiments.
- An orthotropic symmetric model was recommended to predicted bone response and failure.